Comparative Evaluation of Gate Driver and LC-Filter Based dv/dt-Limitation for SiC-Based Motor-Integrated Variable Speed Drive Inverters

MICHAEL HAIDER ⬥, **PASCAL S. NIKLAUS** ⬥ **(Student Member, IEEE), MANUEL MADLENER,**
GWENDOLIN ROHNER ⬥ **(Student Member, IEEE), AND JOHANN W. KOLAR** ⬥ **(Fellow, IEEE)**

Power Electronic Systems Laboratory, Swiss Federal Institute of Technology, 8092 Zurich, Switzerland

CORRESPONDING AUTHOR: PASCAL S. NIKLAUS (e-mail: niklaus@lem.ee.ethz.ch)

Initial results of this article were presented at the IEEE Energy Conversion Congress and Exposition (ECCE USA), Detroit, MI, USA, Oct. 2020.

ABSTRACT Compared to state-of-the-art IGBTs, SiC power semiconductors allow to achieve ever higher system efficiencies and higher power densities in next-generation Variable Speed Drives (VSDs), thanks to their smaller relative chip size, ohmic on-state characteristic and lower specific switching losses resulting in a smaller switching-stage footprint and lower heat sink as well as DC-link capacitor volumes. However, the high slew rate of the switching transitions, an inherent consequence of the low switching losses, represents a major challenge and potentially results in lifetime degrading unequal voltage distribution across the motor windings and bearing currents. This work analytically and experimentally compares different means for dv/dt-limitation, namely, a conventional passive LC-dv/dt-filter and a Gate Driver (GD)-based approach based on increased GD resistances in combination with explicit Miller capacitors, at the example of a 10 kW industrial motor-integrated VSD. For a state-of-the-art dv/dt-limitation of up to 6 V/ns the LC-filter shows lower losses compared to the GD-based limitation. The latter, however, has a higher part-load efficiency and/or lower losses compared to the (roughly) load independent losses in the LC-filter resulting from the dissipation of the energy stored in the filter capacitor within each switching cycle, beneficial for light loads, e.g., $< 40\%$ of rated output power. Next-generation motors with reinforced insulation allow a dv/dt-limitation of up to 15 V/ns. In this case, the GD-based limitation shows lower losses in the whole operating range, since they directly scale with the now smaller overlap of voltage and current resulting from the faster switching transitions. Considering a state-of-the-art motor, finally, a hardware demonstrator of a three-phase VSD employing an LC-filter to limit the dv/dt to 5.6 V/ns is realized, which achieves a full inverter stage power density of 30 kW/dm^3 (497 W/in^3) and an inverter efficiency of $> 99\%$.

INDEX TERMS Gate drivers, permanent magnet motors, pulse width modulation converters, silicon carbide, transmission lines, variable speed drives.

I. INTRODUCTION

Between 40% and 50% of the global energy consumption is attributed to electric motor-driven systems [2], [3], primarily in industrial applications, which motivates an investigation of improvements in energy conversion efficiency, in particular of three-phase VSD inverter systems. In the multi-kW range, state-of-the-art inverters are typically composed of Si IGBTs with antiparallel freewheeling diodes and are operated

at switching frequencies in the range of several kHz to several tens of kHz [4], [5]. SiC MOSFETs are offering an interesting alternative for next-generation VSDs, since they contain internal diodes, hence omitting the need of dedicated external freewheeling diodes, and in contrast to IGBT power devices they do not exhibit a constant forward voltage drop in the on-state, hence offering significantly reduced conduction losses, which is of particular advantage for part-load operation that

often contributes a major share in typical mission profiles of electric motors [6]. Thanks to their high switching speed (high dv/dt and high di/dt) and the significantly lower reverse recovery charge of the internal freewheeling diodes, for the same conduction losses, SiC power semiconductors have a significantly smaller chip area and therefore, lower switching losses [7]. For a given loss budget they can thus be operated at a higher switching frequency up to hundred kHz or more [8], which reduces the required capacitance / size of the DC-link capacitor and increases power density. A minimized functional volume, i.e., a high power density, is particularly important for ever-more popular Integrated Motor Drives (IMDs) where the VSD is placed inside the machine housing and thus must be realized as compact as possible due to space restrictions [9]. A further advantage of IMDs is the absence of long motor cables, which on the one hand are expensive and heavy and on the other hand already for relatively low voltage transition rates of the switched PWM output voltage lead to transmission line effects, e.g., voltage reflections and ringing [10] that increase the insulation stress due to overvoltage at the machine terminals.

A higher switching frequency and accompanying lower volume, however, increases the loss density of the inverter system. Given that typical electric motors have efficiencies in the range of $90 - 95\%$, a required inverter efficiency of typically $> 99\%$ for IMDs is dictated by the thermal design in order to safely dissipate the losses, more than by the overall system efficiency, which is clearly dominated by the motor.

The high switching speed (in particular the high dv/dt) of $20\ldots > 50$ V/ns occurring in SiC MOSFETs imposes various challenges, for example, said transmission line effects typically occurring in state-of-the-art IGBT VSDs with long motor cables can now also occur in IMDs, i.e., even without motor cables [11], [12]. These effects mainly result in an uneven voltage distribution (coil-to-coil and turn-to-turn) within the machine winding, which can drastically reduce the lifetime of the insulation, e.g., due to partial discharge and/or accelerated insulation aging [9], [13]. Moreover, the Common Mode (CM) voltage components with a high dv/dt lead to high bearing currents that reduce the bearing lifetime [14]. While a full sinewave filter would address the aforementioned challenges and thanks to the increased switching frequency in next-generation SiC-based VSDs may be more attractive to implement, it would still significantly impair the inverter power density and would also be a major cost driver. Therefore, it is desired to only implement the absolutely minimum necessary filtering, i.e., to only limit the fast dv/dt voltage transients applied to the motor (a Permanent Magnet Synchronous Motor (PMSM) in the case at hand), e.g., by means of a single-stage LC-dv/dt-filter [15], [16], as shown in Fig. 1. Considering according standards [17], [18], the dv/dt-values (voltage slew rate; measured between 10 % and 90 % of V_{DC} and vice versa) of industrial inverter systems are typically limited to $3\ldots6$ V/ns in order to restrain the aforementioned detrimental effects. However, next-generation electric machines with reinforced motor insulation are projected to
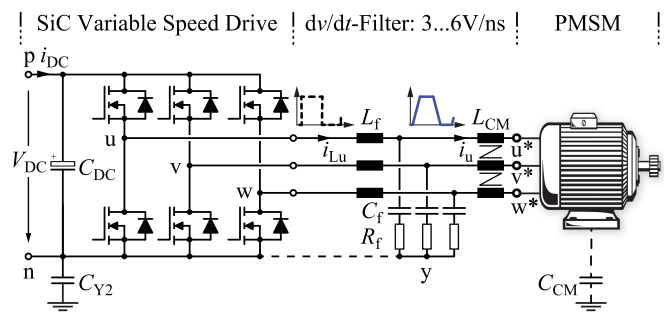

FIGURE 1. Three-phase Variable Speed Drive (VSD) inverter system employing latest SiC MOSFETs that achieve a $dv/dt > 50$ V/ns. To protect the motor isolation, an LC-dv/dt-filter is installed to limit the voltage transition rates to typically $3\ldots6$ V/ns for state-of-the-art motors [1]. The filter capacitor C_f for each phase can be referred to the negative (and/or positive) DC-link rail (dashed line) and thereby the filter is effective for limiting the dv/dt of differential-mode (DM) *and* common-mode (CM) inverter output voltage components. The additional CM choke L_{CM} further limits the CM currents through the bearings arising from the typically relatively large CM capacitance C_{CM} of the machine and moreover reduces radiated electromagnetic emissions.

TABLE 1. Specifications of the Three-Phase IMD Inverter System

Description	Parameter	Value
Max. Mech. Output Power	$P_{M,max}$	10 kW
Nom. Mech. Output Power	$P_{M,nom}$	8 kW
Rated Mechanical Speed	n_M	4000 rpm
Rated Inv. Output Frequency	f_E	333 Hz
DC-Link Voltage	V_{DC}	800 V
Switching Frequency	f_{sw}	16 kHz
Voltage Slew Rate Limit	dv/dt	5 V/ns or 12 V/ns

withstand considerably higher dv/dt-ratings of $10\ldots15$ V/ns. Various dv/dt-limiting/filtering concepts, i.e., active, passive and hybrid approaches, are reported in literature and have been reviewed in [1]. It should be noted that there are also concepts to directly mitigate the overvoltage at the machine terminal and/or the unequal voltage distribution across the winding coils inside the machine by means of small auxiliary circuits in parallel to the first few turns ("smart coils") [19]. These solutions, however, need careful tuning for each specific machine and require additional active components (switches) with driving circuitry.

This article focuses on the two most promising dv/dt-limitation concepts on the VSD side, namely a passive LC-dv/dt-filter employing a single stage LC-filter with diode-clamped damping network (DRC damping) [20], [21] as well as a GD-based dv/dt-limiting concept featuring a Miller feedback capacitor in combination with increased GD resistances [22], [23] for the exemplary case of a 10 kW three-phase IMD employing SiC power semiconductors with the specifications listed in Table 1. It answers the question, which concept is better suited in terms of efficiency and power density for two distinct maximum dv/dt-values of 5 V/ns for state-of-the-art motors and 12 V/ns for future motors and different load scenarios (full-load or part-load operation) by

theoretical and experimental validation. The switching frequency of $f_{sw} = 16\,\text{kHz}$ is just above the audible range and is selected to minimize the switching losses and to facilitate direct comparison to state-of-the-art VSDs implemented with IGBTs.

Section II explains the two considered dv/dt-limiting concepts before Section III introduces the accompanying trade-offs in terms of losses and functional volume. Section IV then analytically compares the two concepts for different dv/dt-values and load conditions and derives a boundary to select the better-suited concept depending on the operating conditions. The calculations are experimentally verified for both investigated concepts and a three-phase VSD inverter system realization suitable for motor integration is presented. Finally, Section V concludes the article.

II. dv/dt-LIMITING CONCEPTS

A. LC-FILTER BASED dv/dt-FILTER

Passive LC-dv/dt-filters are composed of a filter inductor L_f and a filter capacitor C_f, whereas the latter is advantageously referred to the DC-link rails in order to filter CM *and* Differential Mode (DM) voltage components simultaneously (cf. Fig. 2(a)). The resulting phase modular nature facilitates integration, e.g., into power modules. General filter design goals are to limit the dv/dt to a certain maximum value and at the same time to limit the inductor current swing Δi_{Lu} and output voltage overshoot Δv_{u*n} below given boundaries. In this regard, filter damping is essential to avoid overshoot and excessive ringing of the voltage applied to the motor. In the simplest case of a series LCR-filter, damping is implemented with a resistor R_f in series with C_f (cf. Fig. 1) [24], [25], such that the oscillatory transition excited by each switching pulse quickly decays to the steady state, i.e., $v_{u*n} = V_{DC}$ and $i_{Lu} = i_u$. The drawback of this approach is the dependency of the resultant voltage rise time not only on the filter resonance frequency $\omega_0 = 1/\sqrt{L_f C_f}$ but also on the selected quality factor $Q = R_f/Z_f$ (characteristic filter impedance $Z_f = \sqrt{L_f/C_f}$) that also defines the overshoot and is therefore difficult to calculate [1]. Diode-clamped damping networks (DRC damping) [20], [21] as shown in Fig. 2(a) advantageously decouple the dv/dt and the damping. The desired dv/dt defines the voltage transition rise time t_{R0} and fall time t_{F0} (10 % to 90 % of V_{DC} and vice versa) with

$$t_{R0} = t_{F0} = \frac{0.8 \cdot V_{DC}}{dv/dt} \tag{1}$$

and thanks to the disconnected damping network for $0 < v_{u*n} < V_{DC}$ is solely defined by the resonance formed with L_f and C_f (cf. characteristic waveforms in Fig. 2(b)), i.e.,

$$v_{u*n}(t) = V_{DC} \cdot (1 - \cos(\omega_0 t)). \tag{2}$$

Therefrom, the rise time

$$t_{R0} = t\big|_{v_{u*n}(t)=0.9V_{DC}} - t\big|_{v_{u*n}(t)=0.1V_{DC}} \tag{3}$$
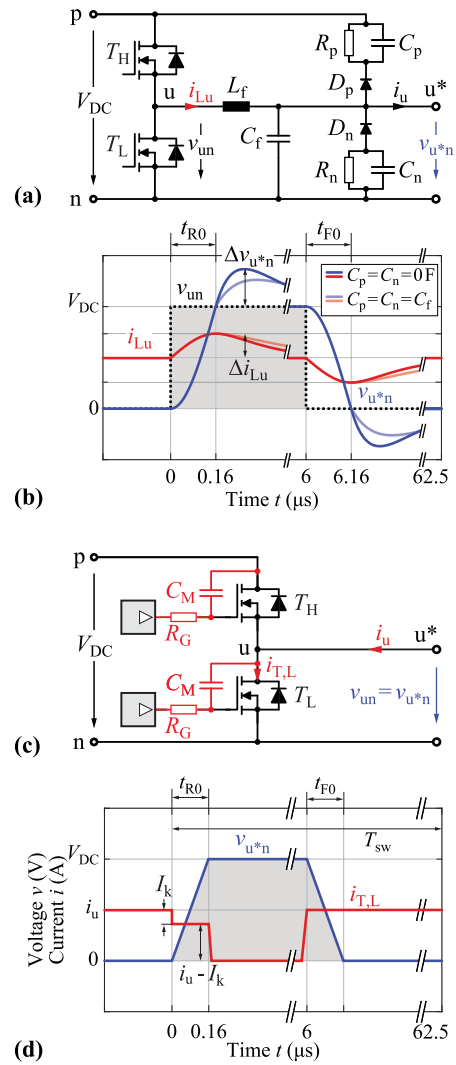

(a)

(b)

(c)

(d)

FIGURE 2. Investigated dv/dt-limiting concepts [1] for phase *u* from Fig. 1. (a) LC-dv/dt-filter with diode-clamped damping network (DRC damping) to limit the inductor peak current and voltage overshoot in phase *u*. (b) Characteristic waveforms of the LC-dv/dt-filter, with the unfiltered switch-node voltage v_{un} (dashed), the filtered output voltage v_{u*n} (blue) and the inductor current i_{Lu} (red) for two cases, with and without additional damping capacitors C_p and C_n, which help to further reduce the voltage overshoot. (c) GD-based dv/dt-limiting with a Miller feedback capacitor C_M and GD resistor R_G (in the actual realization, different R_G values are used for the turn-on and the turn-off switching transition). (d) Zoomed idealized (straight line approximation) view of the voltage v_{u*n} across the low-side transistor (blue) and its corresponding channel current $i_{T,L}$ (red) for a negative instantaneous phase current (i_u indicates the physical current direction) during one switching period $T_{sw} = 1/f_{sw} = 62.5\,\mu s$, indicating the "kink" current, which leads to a slew-rate limited turn-off transition (during t_{R0}). The limited voltage transients of the turn-on and turn-off transitions (during t_{F0} and t_{R0}, both equal 160 ns for a $dv/dt = 5\,\text{V/ns}$ and $V_{DC} = 800\,\text{V}$) are highlighted.

results and finally, the dv/dt can be analytically described as

$$\frac{dv}{dt} = \frac{0.8 \cdot V_{DC}}{(\arccos(0.1) - \arccos(0.9))/\omega_0} = 0.8 \cdot V_{DC} \cdot \frac{\omega_0}{\Omega} \tag{4}$$

with $\Omega := \arccos(0.1) - \arccos(0.9) \approx 1.02$. It therefore only depends on L_f and C_f, which have to be selected accordingly. Considering that the filter is loaded with the motor (i.e., its input impedance in case of an IMD) or even with the motor cable + motor, the filter characteristic becomes load-dependent. It is very difficult to generalize such a setup due to the large variety of different motors and cables. In the case at hand we focus on an IMD (no motor cable) for the PMSM 1FT7084 from Siemens [26], which is a typical example for an industrial 10 kW drive system with specifications as listed in Table 1. In order to be largely independent of the machine loading, the filter output impedance $Z_{o,f}$ must be smaller than the machine input impedance in the frequency range of interest for the considered dv/dt, i.e., around the filter resonance frequency $f_0 = \omega_0/(2\pi)$ [1]. In a typical modulation scheme, only one bridge-leg is switched at a time, which leads to the same voltage step applied to the machine regardless of the switching state changes, i.e., always one phase is switched from 0 V to V_{DC} (or vice versa), while the other two terminals are assumed to be clamped to the negative (or positive) DC-link rail and in addition, considering the worst-case of a direct connection of the negative DC-link rail with PE, i.e., a shorted C_{Y2} (cf. Fig. 1), also to PE. Therefore, the machine impedance seen between, e.g., terminal u and shorted terminals v, w, and *PE* (case) (Z_{U-VWPE}) has to be evaluated and impedance measurements reveal that in the relevant frequency range the PMSM behaves like a capacitance of around 300 pF (cf. **Appendix**). Thus, in order to ensure $Z_{o,f} < Z_{U-VWPE}$ with the worst-case assumption that $Z_{o,f}$ is solely defined by C_f, $C_f \geq 1$ nF is selected (three times larger value). While the semiconductor losses remain unaffected by placing an LC-dv/dt-filter (they still switch with a very high dv/dt in the range of $20\ldots50$ V/ns), the filter capacitor C_f needs to be charged and discharged once every switching period. This translates into an energy loss $E_C = 2 \cdot \frac{1}{2}C_f V_{DC}^2$, independent of the switched current, which is dissipated mainly in the resistors of the damping network. It is thus advisable to select the minimum possible C_f to minimize the filter losses. For a given C_f the filter inductance L_f directly follows from the desired dv/dt using (4), e.g., a dv/dt of 5 V/ns and 12 V/ns requires $L_f = 14\,\mu$H and $L_f = 2.4\,\mu$H, respectively, for $C_f = 1$ nF and $V_{DC} = 800$ V. The filter losses are dissipated in the damping resistors R_p and R_n (cf. Fig. 2(a)), which are selected to achieve critical damping ($Q = 0.5$). The additional capacitors C_p and C_n in parallel to the respective damping resistors do not influence the filter losses but reduce the voltage overshoot Δv_{u*n} at the cost of a prolonged discharging time, as indicated with the dim curves in the characteristic waveforms of Fig. 2(b). The filter inductors must be designed for a peak current $i_{L,pk} = \hat{i}_u + \Delta i_{Lu}$, with the phase current amplitude $\hat{i}_u$ and the inductor current swing $\Delta i_{Lu} = V_{DC}/Z_f$ to charge C_f. Fig. 3(a) exemplary shows the required components to implement one slew-rate limited bridge-leg of the three-phase VSD with a dv/dt-limitation of 5 V/ns realized by means of a passive LC-filter employing DRC damping.
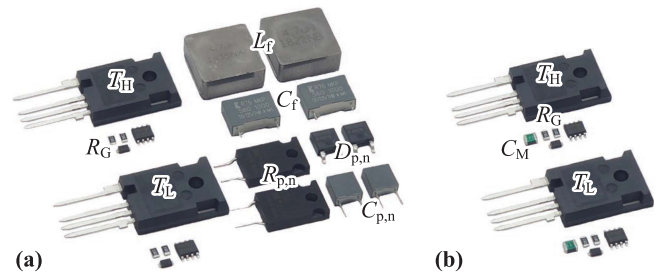

FIGURE 3. Components required to implement a dv/dt-limited SiC bridge-leg employing (a) a passive $LC-$ filter with DRC damping and (b) a GD-based limitation with increased GD resistances and explicit Miller feedback capacitor C_M.

B. GATE DRIVER BASED dv/dt-LIMITATION

The apparent drawback of a passive dv/dt-limiting filter is the additional volume and cost of the filtering elements (though, they are considerably smaller compared to a full sinewave filter). Alternatively, the dv/dt of the voltage applied to the machine can be limited *directly* via the GD voltage, which only requires very small passive elements and therefore, has a negligible contribution to the component volume, as depicted in Fig. 3(b). Different realizations either limit the gate time constant, e.g., by using different gate resistance values [27], [28], [29] or by implementing closed-loop gate control [30], [31]. An alternative implementation not only modifies the gate time constant but also artificially increases the gate-to-drain capacitance C_{GD} of the MOSFET with an external so-called Miller capacitance C_M between drain and gate (in the range of few pF, hence very small) as shown in Fig. 2(c), to inherently slow down the dv/dt transient and thereby potentially gains advantages in terms of losses. A detailed analysis of the resulting MOSFET turn-on and turn-off transitions is carried out in [23] and reveals that both are equally slowed down by the combination of gate resistance R_G and C_M. This is indicated in Fig. 2(d), which shows a zoomed view of one switching period T_{sw} during the fundamental frequency period $T_E = 1/f_E$ where the momentary phase current i_u (and thus switched current) is negative (i_u in Fig. 2(c) indicates the physical current direction).

The slowed down voltage transitions lead to a voltage-current overlap and hence to increased switching losses. The additional overlap losses in the (ideally lossless) turn-off transition (during t_{R0} for a negative switched current of the low-side transistor T_L) have been comprehensively discussed in [22] and are attributed to the voltage-current overlap resulting from a residual current in the channel of T_L while its C_{GD}, C_M and the drain-to-source capacitance C_{DS} are charged (and the high-side transistor T_H's C_{DS}, C_{GD} and C_M are discharged). Assuming for simplicity no external Miller capacitor ($C_M = 0$ pF) and a certain switched current i_u, the resonant Zero Voltage Switching (ZVS) transition would charge C_{GD} of T_L with a current $i_{C_{GD}}$ determined by the current divider $C_{GD}/(C_{DS} + C_{GD})$ (and similarly charge

C_{DS} of T_L with a current determined by $C_{DS}/(C_{DS} + C_{GD})$), which together with the current discharging the gate-to-source capacitance C_{GS} equals the total gate current i_G. The latter is limited to $i_{G,max} = (v_{th} + |V_{GD,n}|)/R_{G,off}$ by the GD as a function of the MOSFET threshold voltage v_{th}, the negative GD voltage $V_{GD,n}$ and the turn-off gate resistance $R_{G,off}$ (composed of the externally placed resistance and a GD-internal part representing the limited current drive capability). For switched currents above a certain limit I_k (the so-called "kink" current [22]) and considering only the capacitive current divider, $i_{C_{GD}}$ would need to exceed $i_{G,max}$, which is not possible. Therefore, a certain residual current $(i_u - I_k)$ continues to flow in the MOSFET channel, causing said overlap losses. As derived in [22], the limit I_k is defined as the switched current $i_u = I_k$ that is entirely split between C_{GD} (and C_M in parallel) of T_L and the parallel combination of C_{DS} of T_L, C_{DS} of T_H and C_{GD} and C_M of T_H (current divider) and where $i_{C_{GD}} = i_{G,max}$, i.e.,

$$I_k = \frac{v_{th} + |V_{GD,n}|}{R_{G,off}} \cdot 2 \cdot \left(1 + \frac{C_{dQ,DS}}{C_{dQ,GD} + C_M}\right), \quad (5)$$

assuming a very high MOSFET transconductance g_m. To account for the non-linear capacitances C_{DS} and C_{GD} with changing voltage, $C_{dQ,DS}$ and $C_{dQ,GD}$ denote the charge-equivalent linear capacitances for a voltage change between 10 % and 90 % of V_{DC} (or between 90 % and 10 % of V_{DC}), i.e., the voltage range $\Delta v = 0.8 \cdot V_{DC}$ in which the dv/dt is evaluated. The factor of two in (5) accounts for the charging/discharging of C_{DS}, C_{GD} and C_M of the high-side *and* low-side transistors during the ZVS transition. $I_k = \{6.3\,A, 18.2\,A\}$ result for the utilized component values and the two considered dv/dt-limiting values of 5 V/ns and 12 V/ns, respectively (cf. Table 2), which accounts for $\approx 24\,\%$ and $\approx 70\,\%$ of the phase current amplitude at full output power (cf. (11)). Therefore, it is important to consider the effect of I_k on the resulting semiconductor losses as it is done in Section III-C.

From I_k follows now directly the *desired* reduced turn-off voltage transition rate (straight-line approximation)

$$\left.\frac{dv}{dt}\right|_{off} = \frac{I_k}{2 \cdot (C_{dQ,DS} + C_{dQ,GD} + C_M) + C_{par}}, \quad (6)$$

as further derived in [22] and again using the charge-equivalent capacitances. Moreover, C_{par} includes various parasitic capacitances, e.g., from the PCB layout or the heat sink. Combining (5) and (6) and neglecting C_{par}, the simplified expression

$$\left.\frac{dv}{dt}\right|_{off} = \frac{v_{th} + |V_{GD,n}|}{R_{G,off} \cdot (C_{dQ,GD} + C_M)} \quad (7)$$

results. Equation (7) clearly illustrates that for a given GD supply voltage, the dv/dt is defined by the product of GD resistance and (total) Miller capacitance and therefore, multiple combinations result in the same dv/dt. Note that (5) to (7) assume C_M and C_{GD} connected in parallel, i.e., the

internal gate resistance of the power semiconductor is assumed zero. Furthermore, it has to be noted that the dv/dt in (7) slightly increases for switched currents $i_u > I_k$, since the gate-to-source voltage during the voltage transition equals the Miller-plateau voltage $v_M = v_{th} + (i_u - I_k)/g_m$ (MOSFET transconductance g_m), slightly raising the maximum possible gate current and thus accelerating the charging of C_{GD} and C_M. Given the typically very high g_m of power MOSFETs ($g_m = 53\,S$ for the device used here, C3M0016120K, cf. Table 2) this effect is not significant.

The turn-on transition of T_L (during t_{F0} in Fig. 2(d)), again assuming a negative phase current and thus a negative switched current i_u, is a Hard Switching (HSW) transition, which causes overlap losses, because after turn-off of the high-side switch T_H, i_u commutates in its freewheeling diode, i.e., V_{DC} remains across the low-side transistor T_L, and only after an enforced dead time i_u commutates to the channel of T_L (turn-on of T_L). With increasing gate resistance and/or Miller capacitance the maximum current to charge C_{GD} (and C_M) of T_H and to discharge C_{GD} (and C_M) of T_L is limited by the GD resulting in increased overlap losses due to the *desired* slowed down turn-on voltage transition

$$\left.\frac{dv}{dt}\right|_{on} = \frac{V_{GD,on} - v_{th}}{R_{G,on} \cdot (C_{dQ,GD} + C_M)}, \quad (8)$$

with the positive GD drive supply voltage $V_{GD,p}$ and the turn-on gate resistance $R_{G,on}$.

Resulting from (7) and (8), a certain dv/dt can be achieved with different combinations of $R_{G,on}$ and $R_{G,off}$ and C_M, for example a slew rate limit of 10 V/ns could be achieved with $C_M = 50\,pF$, $R_{G,on} = 9.5\,\Omega$ and $R_{G,off} = 11.0\,\Omega$ or with $C_M = 0\,pF$ (only the device-internal C_{GD} is effective), $R_{G,on} = 30.1\,\Omega$ and $R_{G,off} = 24.3\,\Omega$ [23]. Measurements in [23] show, however, that the losses do not significantly change for different combinations, thus in the interest of simplicity, $C_M = 0\,pF$ can be chosen and the dv/dt is set entirely with the GD resistance. Actual dv/dt, $R_{G,on}$, $R_{G,off}$ and C_M values for the utilized system are indicated in Table 2. Note that changing the gate resistance directly changes the gate time constant $\tau_{GS,on} = R_{G,on} \cdot C_{GS}$ (and $\tau_{GS,off} = R_{G,off} \cdot C_{GS}$), which influences the time for the gate-to-source voltage to rise from the threshold voltage v_{th} to the Miller-plateau voltage $v_M = v_{th} + i_u/g_m$ during the turn-on transition (and vice versa to fall from the Miller plateau to v_{th} during the turn-off transition) and therefore leads to a finite current slew rate di/dt (indicated in Fig. 2(d)). Calculations with the utilized device parameters (cf. Table 2) verify that the current rise and fall times are still more than one order of magnitude faster compared to the voltage transition times t_{R0} and t_{F0} and are hence neglected.

III. LOSS AND VOLUME CALCULATION
Both presented dv/dt-limiting concepts cause additional losses, either due to capacitor charging/discharging (filter capacitor C_f of the LC-dv/dt-filter) or overlap losses (GD-based limitation), and further contribute a certain volume, e.g., of

additional passive elements and of the required heat sink to dissipate the additional losses. Since the goal is to select the best-suited dv/dt-limiting approach based on loss and volume considerations, approximative quantitative loss and volume models are derived in the following. It is important to discriminate the additional losses/volumes caused by dv/dt-limiting concepts from losses that are inherently present, including the capacitive losses occurring due to charging/discharging of the parasitic machine capacitances. These losses act as loss offset and in a first approximation are assumed to not change if the voltage slew rate is limited by either of the concepts.

A. INVERTER OUTPUT POWER

At rated mechanical rotational speed $n_M = 4000$ rpm ($\omega_M = 2\pi \cdot n_M/60 = 2\pi \cdot 67$ Hz) and with the voltage constant $k_V = \frac{V_{ll,rms}}{n_M} = 83$ mV/rpm and $p = 5$ pole pairs [26], the induced motor winding (phase) voltage has an amplitude $\hat{v}_{ind}$ and an electrical angular frequency ω_E

$$\hat{v}_{ind} = \sqrt{\frac{2}{3}} \cdot k_V \cdot n_M = 270 \text{ V}, \qquad (9)$$

$$\omega_E = p \cdot \omega_M = 2\pi \cdot 333 \text{ Hz}, \qquad (10)$$

in accordance with [1]. The resulting maximum phase current amplitude at full power ($P_{M,max} = 10$ kW), i.e., at full torque of $T_{M,max} = 23.8$ Nm, is

$$\hat{i}_{u,max} = \sqrt{2} \cdot \frac{T_{M,max}}{k_T} = 25.9 \text{ A} \qquad (11)$$

with the machine torque constant $k_T = \frac{T_M}{I_{l,rms}} = 1.3$ Nm/A [26]. Typical mission profiles of industrial drive systems are largely containing part-load operation, e.g., a reduced nominal torque of $T_{nom} = 0.8 \cdot T_{M,max} = 19$ Nm ($\hat{i}_{u,nom} = 20.7$ A) at nominal rotational speed, which justifies investigation of the optimally suited dv/dt-limiting concept for such a part-load case. Unsurprisingly, combining (9) with (11) results in the maximum mechanical output power of $P_{M,max} = 10$ kW and when using $T_{M,nom}$ instead of $T_{M,max}$, in $P_{M,nom} = 8$ kW. The output power of each inverter phase can be expressed with

$$P_u = \frac{1}{\sqrt{2}} M \frac{V_{DC}}{2} \cos(\varphi) \cdot \frac{\hat{i}_u}{\sqrt{2}} = \frac{1}{4} M V_{DC} \cos(\varphi) \cdot \hat{i}_u, \quad (12)$$

where $M V_{DC}/2$ denotes the amplitude $\hat{v}_u$ of the inverter phase output voltage (modulation depth M). Assuming the load current to be in-phase with the induced motor voltage v_{ind}, in a complex phasor representation, the projection of the inverter output voltage phasor $\underline{\hat{v}}_u$ on the real axis, i.e., $\underline{\hat{v}}_u \cdot \cos(\varphi)$, corresponds to the induced motor voltage $\underline{\hat{v}}_{ind}$. According to (9), the amplitude of this projected voltage $\hat{v}_{ind} = M V_{DC}/2 \cdot \cos(\varphi)$ is directly related to the rotational speed and thus constant and load-independent (typically, there is a superordinate speed controller that regulates n_{rpm} to the desired value). For $n_{rpm} = 4000$ rpm and the given machine parameters [26], $M\cos(\varphi) = 0.68$ [1] and therefrom P_u can be calculated straight-forward.

B. LOSSES AND VOLUME OF THE PASSIVE LC-dv/dt-FILTER

In a passive LC-dv/dt-filter the power semiconductors themselves are switching with a typically very high dv/dt and switching loss models obtained from device characterization (e.g., thermally measured [32]) with quadratic fitting coefficients k_0, k_1 and k_2 can be used. For a purely sinusoidal switched current, i.e., no current ripple (justified with the relatively large machine inductance), the semiconductor losses per phase (half-bridge losses $P_{l,HB}$) for a certain $\hat{i}_u$ then equal

$$P_{l,HB} = \frac{1}{2} R_{DS,on} \hat{i}_u^2 + f_{sw}\left(k_0 + \frac{2}{\pi} k_1 \hat{i}_u + \frac{1}{2} k_2 \hat{i}_u^2\right). \quad (13)$$

C3M0016120K 1200 V SiC power semiconductors ($R_{DS,on} = 16$ mΩ at $T_j = 25$ °C) are found to minimize the total semiconductor losses (conduction and switching) in the given application with part-load operation at $P_{M,nom} = 8$ kW ($\hat{i}_u = 20.7$ A) [1]. Their calorimetrically measured switching loss coefficients are $k_0 = 312.2$ µJ, $k_1 = 7.2$ µJ/A and $k_2 = 120.8$ nJ/A^2 (cf. Table 2). A junction temperature $T_j = 100$ °C is assumed to calculate the conduction losses, i.e., $R_{DS,on,100°} = 20$ mΩ [33].

Additional loss components are the charging/discharging losses $P_{C_f} = C_f V_{DC}^2 f_{sw}$ of the filter capacitance C_f, which are dissipated mainly in the resistors of the DRC damping network, and the filter inductor conduction losses $P_{L_f} = \frac{1}{2} R_{L_f} \hat{i}_u^2$ (neglecting core losses due to the low fundamental frequency and the generally low current ripple given the large motor winding inductance; further neglected are hence the conduction losses arising from the current ripple and the contribution of the current pulse Δi_{Lu} to the total RMS current, which is found to be negligible). In total, the per-phase losses of a bridge-leg featuring a passive LC-dv/dt-filter are

$$P_{l,f} = P_{l,HB} + P_{C_f} + P_{L_f}. \qquad (14)$$

Neglecting the filter capacitor volume (high capacitance density), only the volume of the heat sink to dissipate the filter losses and the filter inductor volume have to be considered. The former can be approximated using the so-called *Cooling System Performance Index (CSPI)* [34] with a typical CSPI of 20 W/(K · dm^3), an assumed heat sink temperature of $\vartheta_{HS} = 85$ °C and an ambient temperature $\vartheta_{amb} = 40$ °C using

$$R_{th,HS,f} = \frac{\vartheta_{HS} - \vartheta_{amb}}{3 \cdot P_{l,f}}, \qquad (15)$$

$$V_{HS,f} = \frac{1}{CSPI \cdot R_{th,HS,f}} \propto P_{l,f}. \qquad (16)$$

As derived in Section II-A, the filter inductance directly follows from the selected dv/dt limit. For the given application the maximum phase RMS current equals $I_{u,rms,max} = 18.3$ A and the peak current follows from $\hat{i}_{u,max}$ in (11) and the additional current peak Δi_{Lu} to charge C_f. Even though the VSD is primarily operating in part-load, the filter inductor has to be designed for full-load, i.e., for an RMS current rating $I_{rated} \geq I_{u,rms,max}$ (as mentioned above, the contribution of the current pulse Δi_{Lu} on the total RMS current is found to be
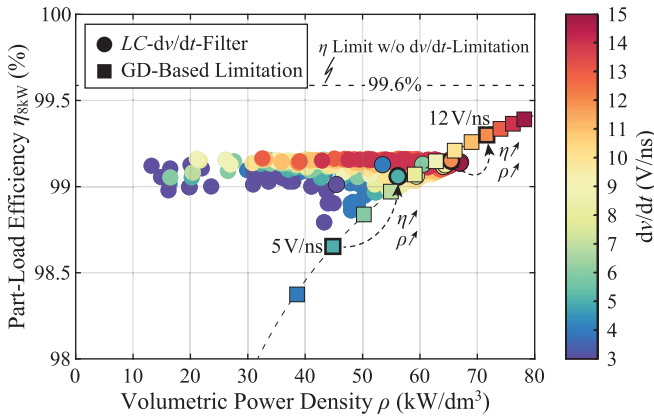
FIGURE 4. $\eta\rho$-Pareto optimization for a 10 kW three-phase SiC-VSD showing the trade-off between achievable power density ρ and part-load efficiency $\eta_{8\,kW}$ at $P_{M,nom} = 8$ kW for the damped passive *LC*-dv/dt-filter (dots) and the GD-based dv/dt-limitation (squares) for different dv/dt limits between 3 V/ns and 15 V/ns, a maximum phase current $\hat{i}_{u,max} = 25.9$ A and a fixed *LC*-filter capacitance $C_f = 1.12$ nF.

negligible) and for a saturation current $i_{sat} \geq \hat{i}_{u,max} + \Delta i_{Lu}$. The dots in the $\eta\rho$-Pareto optimization in Fig. 4 show the design trade-off for the *LC*-dv/dt-filter for dv/dt limits between 3 V/ns and 15 V/ns with the total VSD power density ρ and the part-load efficiency $\eta_{8\,kW}$ at $P_{M,nom} = 8$ kW. The filter capacitance C_f is fixed to a value of 1.12 nF (two 560 pF capacitors in parallel, connected to the positive and negative DC-link rail) *a)* to fulfill the filter output impedance criterion ($Z_{o,f} < Z_{M,U-VWPE}$) and *b)* to minimize the (load independent) losses P_{C_f}. Generally, high dv/dt limits are accompanied by a higher power density due to the smaller L_f. At the same time, a low L_f results in lower conduction losses P_{L_f}, hence also the efficiency improves (the other loss components in (14) are independent of the selected dv/dt limit). For IMDs, ideally the design with the highest power density is chosen to facilitate integration (highlighted with black circles for each dv/dt).

C. LOSSES AND VOLUME OF THE GATE DRIVER BASED dv/dt-LIMITATION

The GD-based dv/dt limitation leads to increased switching losses $E_{sw,GD}$, which for a switched current i_u have been derived in [23] as

$$E_{sw,GD} = k_0 + k_{on} \cdot i_u + \begin{cases} 0 & \text{if } i_u \leq I_k \\ k_{off} \cdot (i_u - I_k) & \text{if } i_u > I_k \end{cases} \quad (17)$$

with $k_{on} = \frac{k_{WF}}{2} V_{DC}^2 / \frac{dv}{dt}$ and $k_{off} = \frac{1}{2} V_{DC}^2 / \frac{dv}{dt}$. The factor $k_{WF} = 1.35$ is empirically determined and corrects inaccuracies due to the straight-line approximation of the voltage transient between 10% and 90% of V_{DC}, only of a concern for the turn-on transition [23]. Note that the term k_2 considering losses scaling quadratically with the switched current is neglected, since the linearly scaling loss contribution arising from the limited dv/dt is clearly dominating the overlap losses. Moreover, the ZVS losses attributed to the

resonant charging/discharging of the transistor output capacitance $C_{oss} = C_{DS} + C_{GD}$ are neglected.

Evaluating (17) for a sinusoidal phase current with amplitude $\hat{i}_u$, including the semiconductor conduction losses and again neglecting the current ripple, the total per-phase losses $P_{l,GD}$ for the GD-based dv/dt-limitation are

$$P_{l,GD} = \frac{1}{2} R_{DS,on,100°} \hat{i}_u^2 + f_{sw} \left(k_0 + \frac{2}{\pi} k_{on} \hat{i}_u \right)$$

$$+ \begin{cases} 0, & \hat{i}_u \leq I_k \\ \frac{2 f_{sw} k_{off}}{\pi} \left[\sqrt{\hat{i}_u^2 - I_k^2} - I_k \arccos\left(\frac{I_k}{\hat{i}_u}\right) \right], & \hat{i}_u > I_k \end{cases}$$

$$(18)$$

where the values of I_k for the two cases with a dv/dt-limitation of (I) 5 V/ns and (II) 12 V/ns are listed in Table 2. For a given $\hat{i}_u$, $P_{l,GD}$ scales inversely proportional with the selected voltage slew rate dv/dt, which is intuitively clear that faster voltage transients lead to lower overlap losses.

Since the volume of the gate resistor and additional Miller capacitor is negligible (cf. Fig. 3(b)), consequently, only the heat sink volume has to be considered, which can be calculated with (15) and (16), replacing $P_{l,f}$ with $P_{l,GD}$ (cf. Fig. 7). The squares in Fig. 4 nicely show the trend of higher efficiency at higher voltage slew rates. Moreover, given the direct relation between losses and (heat sink) volume, there is no Pareto front and/or Pareto-optimal design but more efficient designs are automatically more compact. If no dv/dt-limiting would be employed, the losses would be solely defined by the characteristics of the utilized power semiconductor (conduction and switching losses $P_{l,HB}$ according to (13)) and for the given specifications result in an efficiency limit of $\eta_{max,8\,kW} = 99.6\%$ (indicated with the dashed line in Fig. 4) to which the GD-based dv/dt-limiting approach converges for very high slew-rate limits.

IV. COMPARATIVE EVALUATION

Having defined the inverter loss and volume models considering both dv/dt-limiting approaches, the question therefore arises, which of the two concepts should be selected to limit the dv/dt of a three-phase VSD inverter system with a certain phase current amplitude $\hat{i}_u$ to a specific value (e.g., 5 V/ns for state-of-the-art electric motors or 12 V/ns for future motors with reinforced insulation). To not only theoretically but also experimentally verify the analyses, a characteristic three-phase SiC-based VSD to be integrated into a motor housing is designed and constructed as depicted in Fig. 5, in accordance with the specifications from Table 1. The VSD is equipped with a DRC-damped passive *LC*-filter for dv/dt-limitation but could alternatively also be realized without the filter as GD-based dv/dt-limitation. Two PCBs are vertically stacked to facilitate a compact and phase-modular realization. On the power PCB, besides the power semiconductors (16 mΩ, 1200 V SiC MOSFETs),

TABLE 2. Components and Parameters of the Hardware Realization of the Three-Phase SiC-Based VSD With a Voltage Slew Rate of (I) 5 V/ns and (II) 12 V/ns for Both Considered dv/dt-Limitation Concepts

| Parameter	Value	Part
Power Semiconductor	1.2 kV, 16 mΩ, SiC	C3M0016120K
$k_0 = 312.2\,\mu$J,	$k_1 = 7.2\,\mu$J/A,	$k_2 = 120.8$ nJ/A^2
$v_{th} = 2.5$ V,	$g_m = 53$ S	$R_{DS,on,100°} = 20$ mΩ
$C_{dQ,GD} = 16$ pF	$C_{dQ,DS} = 320$ pF	
Gate Driver	±6 A	1EDI60N12AF
Filter Capacitor C_f	1.12 nF	2× R76QF056050H0J
Damping Cap. $C_{p,n}$	10 nF	R79MC2100AA40J
Clamping Diode $D_{p,n}$	1.2 kV, 5 A, SiC	IDM05G120C5
Filter Inductor L_f (I)	11.2 μH	2× SRP1770TA-5R6M
Damp. Res. $R_{p,n}$ (I)	15 Ω	PWR221T-50-15R0J
Filter Inductor L_f (II)	1.8 μH	CMLS136E-1R8MS
Damp. Res. $R_{p,n}$ (II)	6 Ω	PWR221T-50-6R00F
Miller Capacitor C_M	0 pF	
$R_{G,on}$ / $R_{G,off}$ (I)	56 Ω / 43 Ω	
$R_{G,on}$ / $R_{G,off}$ (II)	15 Ω / 15 Ω	
Pos. GD Sup. $V_{GD,p}$	+15 V	
Neg. GD Sup. $V_{GD,n}$	−4 V	
I_k (I)	6.3 A	(calculated with (5))
I_k (II)	18.2 A	(calculated with (5))
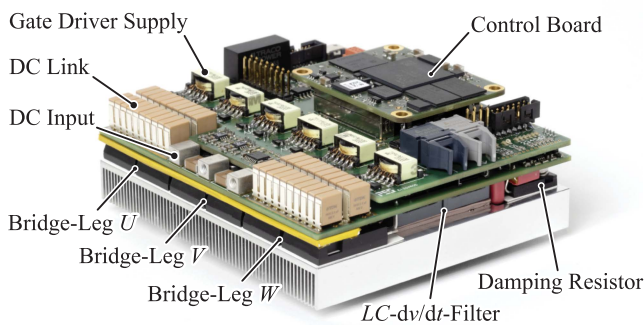
FIGURE 5. Photo of the ultra-compact 10 kW SiC-based three-phase VSD featuring a damped *LC*-dv/dt-filter to limit the voltage slew rate to a nominal value of 5.6 V/ns, i.e., suitable for state-of-the-art electric machines. The most important building blocks are labeled.

the *LC*-dv/dt-filter as well as voltage and current measurements are located. Table 2 lists the important component values and parameters for a nominal voltage slew rate of (I) 5 V/ns and (II) 12 V/ns. The power semiconductors as well as the filter inductors and damping resistors are thermally attached to a thin-fin heat sink with forced cooling. The overall system dimensions are 100 mm × 90 mm × 37 mm (3.94 in. × 3.54 in. × 1.46 in. [L × W × H]; including the control board featuring a Field-Programmable Gate Array (FPGA) and the heat sink), which corresponds to a total boxed volume of $V_{boxed} = 0.333$ dm^3 (20.3 in^3) and thereby a power density of 30 kW/dm^3 (493 W/in^3). The low inverter volume greatly facilitates integration directly into the machine, in which case the heat sink that contributes approximately one third of the total volume (height of 12 mm [0.47 in.], 0.108 dm^3 [6.56 in^3]) could potentially be omitted, if the machine housing would be used for passive cooling of the inverter [35]. Moreover, the control board - currently placed as external module and included in the boxed volume - could
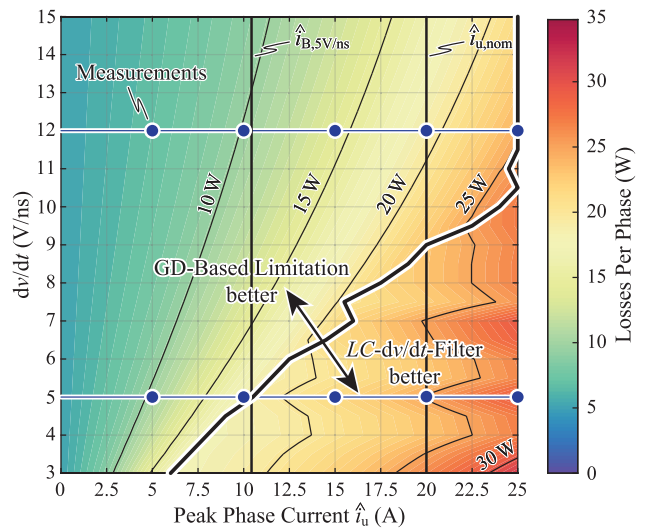

FIGURE 6. Per-phase losses of the loss-optimal dv/dt-limiting concept for a dv/dt-limit between 3 V/ns and 15 V/ns and phase current amplitudes $\hat{i}_u \in [0\,A, 25\,A]$ (part-load and full-load operation). The thick black line depicts the boundary below which the *LC*-dv/dt-filter has lower losses compared to the GD-based limitation. In case of the *LC*-dv/dt-filter, $C_f = 1.12$ nF and L_f is always chosen for $\hat{i}_u = 25.9$ A (full-load).

be fully integrated, enabling a pure inverter power density of roughly 61 kW/dm^3 (1000 W/in^3).

A. PER-PHASE LOSS COMPARISON

To promote motor integration of the inverter, the most compact design of the *LC*-dv/dt-filter is selected from the Pareto front in Fig. 4. Compared to the most efficient (lowest loss) design, the loss penalty is relatively low, whereas considerable volume benefits are apparent. Hence, a single Pareto-optimal filter design results for each dv/dt value for the damped *LC*-dv/dt-filter approach (highlighted with black circles in Fig. 4), which is compared to the GD-based limitation in terms of per-phase losses. Fig. 6 shows the calculated per-phase losses for both limiting approaches under full- and part-load operation ($\hat{i}_u \in [0\,A, \ldots, 25\,A]$ with the *LC*-dv/dt-filter always designed for $\hat{i}_u = \hat{i}_{u,max} = 25.9$ A) for different voltage slew rates dv/dt from 3 V/ns to 15 V/ns. For each combination of $\hat{i}_u$ and dv/dt, the losses of the better-performing approach are depicted. There exists a clear boundary between the *LC*-dv/dt-filter and the GD-based limitation (thick black line), where the former is best-suited for slow transitions at high $\hat{i}_u$ and the latter is ideally used for higher dv/dt values. In particular for dv/dt > 11 V/ns the GD-based limitation leads to lower losses (< 25 W per phase) for full- and part-load operation. For lower dv/dt values there exists a certain boundary current amplitude $\hat{i}_B$ below which the GD-based dv/dt-limitation outperforms the *LC*-dv/dt-filter thanks to its lower part-load losses, e.g., $\hat{i}_{B,5\,V/ns} = 10.5$ A for a voltage slew rate dv/dt = 5 V/ns, since the filter has always a constant loss offset of $P_{C_f} = 11.5$ W for $C_f = 1.12$ nF, $V_{DC} = 800$ V, $f_{sw} = 16$ kHz (dominant over the inductor conduction losses P_{L_f}). Conversely, for part-load operation with $\hat{i}_{u,nom} = 20$ A,
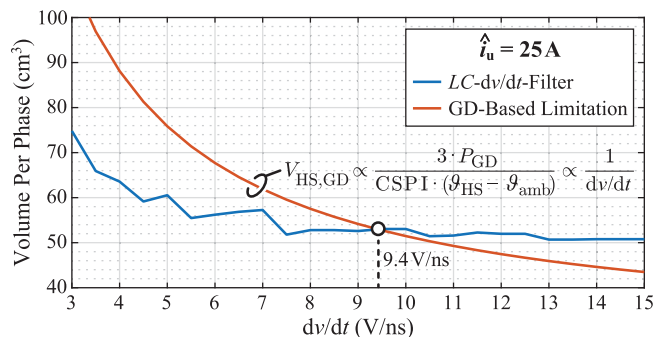
FIGURE 7. Volume comparison of one phase of the three-phase VSD for the *LC*-dv/dt-filter (blue) and the GD-based limitation (orange) for the full-load phase current amplitude $\hat{i}_u = 25\,A$.

the *LC*-dv/dt-filter outperforms the GD-based limitation for voltage slew rates below 9 V/ns because the losses of the latter scale inversely proportional to the dv/dt and thus exceed the constant P_{C_f} losses of the former. Therefore, in theory, a boundary line parametrization $\hat{i}_{B,dv/dt} = \alpha \cdot dv/dt$ with $\alpha = $ const. would be expected. The deviation from this linear relation results from the selection of discrete filter inductors from commercially available components, which leads to discontinuities in the *LC*-dv/dt-filter losses.

B. PER-PHASE VOLUME COMPARISON

A similar boundary is found in Fig. 7 when comparing the functional volume of the two limiting concepts (blue and orange lines for the *LC*-dv/dt-filter and GD-based limitation, respectively) for the maximum phase current amplitude $\hat{i}_{u,max} = 25.9\,A$ (part-load operation does not change the volume, since the VSD must be designed to handle the full power of $P_{M,max} = 10\,kW$). For voltage slew rates above 9.4 V/ns the GD-based dv/dt-limitation can be realized with a lower volume (i.e., lower heat sink volume due to the lower losses with the direct relationship via the CSPI, cf. (16)), whereas in case of the *LC*-dv/dt-filter there is always a certain volume offset given by the filter inductors, which of course can be realized more compact for small inductance L_f (high dv/dt), but the volume reduction saturates due to mechanical constraints (current carrying conductors, minimum core thickness, etc.). The discontinuities in case of the *LC*-dv/dt-filter again result from discrete component selection.

C. EXPERIMENTAL VERIFICATION

To experimentally verify the occurrence of the above discovered boundary, the occurring per-phase losses have been measured on the hardware prototype equipped with either of the two described dv/dt-limiting concepts. The *LC*-dv/dt-filter is realized with $C_f = 1.12\,nF$ (two R76QF056050H0J capacitors in parallel, one connected to the positive and one to the negative DC-link rail) and $L_f = 11.2\,\mu H$ (two SRP1770TA-5R6M inductors in series) or with $C_f = 1.12\,nF$ and $L_f = 1.8\,\mu H$ (CMLS136E-1R8MS) for a nominal dv/dt of 5.6 V/ns and 14 V/ns, respectively. Note that realizing C_f with

two capacitors connected to the positive and negative DC-link rail does not influence the total energy dissipation, but results in a more symmetric layout and thus more symmetric (parasitic) ringing conditions. In both cases (dv/dt of 5.6 V/ns and 14 V/ns), the damping network is composed of two 10 nF capacitors C_p and C_n and implements critical damping with $R_p = R_n = \frac{1}{2}\sqrt{\frac{L_f}{C_f + C_p}}$ (C_p denotes the additional damping capacitance in parallel to the damping resistor, cf. Fig. 2(a)). SiC Schottky diodes with low capacitive charge (24 nC, $\approx 0.3\,W$ losses for $V_{DC} = 800\,V$ and $f_{sw} = 16\,kHz$) and low leakage current (12 μA) are used for D_p and D_n (IDM05G120C5). Due to component tolerances, additional parasitic capacitances and inductances (PCB, connections), finally, the desired voltage slew rates of 5 V/ns and 12 V/ns result (cf. Table 1). Note that for a smaller L_f (higher dv/dt) the impact of parasitic inductances and capacitances is more pronounced (larger deviation of the actual dv/dt from the nominally set value) due to the small nominal value of L_f.

The GD-based limitation is implemented with increased gate turn-on and turn-off resistances of $R_{G,on}/R_{G,off} = 56\,\Omega/43\,\Omega$ and $15\,\Omega/15\,\Omega$ ($C_M = 0\,pF$) for a dv/dt of 5 V/ns and 12 V/ns, respectively (cf. Table 2). Using (5) with $v_{th} = 2.5\,V$, $V_{GD,n} = -4\,V$, $C_{dQ,DS} = 320\,pF$ and $C_{dQ,GD} = 16\,pF$ the "kink" current is $I_k = 6.3\,A$ (5 V/ns) and $I_k = 18.2\,A$ (12 V/ns) for the two cases.

Fig. 8 shows (a) the calculated and measured efficiency and (b) the per-phase losses for dv/dt = 5 V/ns (calculated: dotted lines; measured: circles) and for dv/dt = 12 V/ns (calculated: continuous lines; measured: diamonds) for the *LC*-dv/dt-filter (blue) and the GD-based limitation (orange) for phase current amplitudes $\hat{i}_u = \{5\,A, 10\,A, 15\,A, 20\,A, 25\,A\}$. These operating points are also indicated in Fig. 6. The losses are measured electrically with a precision power analyzer (Yokogawa WT3000) and show good alignment with the calculations, in particular in case of the GD-based limitation, whereas in case of the *LC*-dv/dt-filter and for low $\hat{i}_u$ a certain mismatch is observed. This is primarily explained with the simplified assumption of zero current ripple in the calculation, essentially overestimating the switching losses at low currents (and hence the calculated total losses), since in practice more Partial-Hard Switching (PHSW) and Soft Switching (SSW) transitions occur, which generate lower losses compared to the assumed HSW transitions. In case of the GD-based limitation this effect is less severe, since also the PHSW and SSW transitions lead to overlap losses (for $\hat{i}_u > I_k$).

As expected from the observations in Fig. 6 based on calculated losses, for a dv/dt of 12 V/ns the GD-based limitation is always more efficient (lower losses) compared to the *LC*-dv/dt-filter, e.g., for the nominal phase current $\hat{i}_{u,nom} = 20.7\,A$ the measured losses are 20.5 W with the GD-based limitation and 23.6 W with the *LC*-dv/dt-filter. For a voltage slew rate dv/dt = 5 V/ns, the boundary current $\hat{i}_{B,5\,V/ns}$ is verified, i.e., for currents $\hat{i}_u > 10.5\,A$ the *LC*-dv/dt-filter has lower losses than the GD-based limitation (27.6 W versus 36 W for $\hat{i}_{u,nom}$). The filter losses do not significantly change
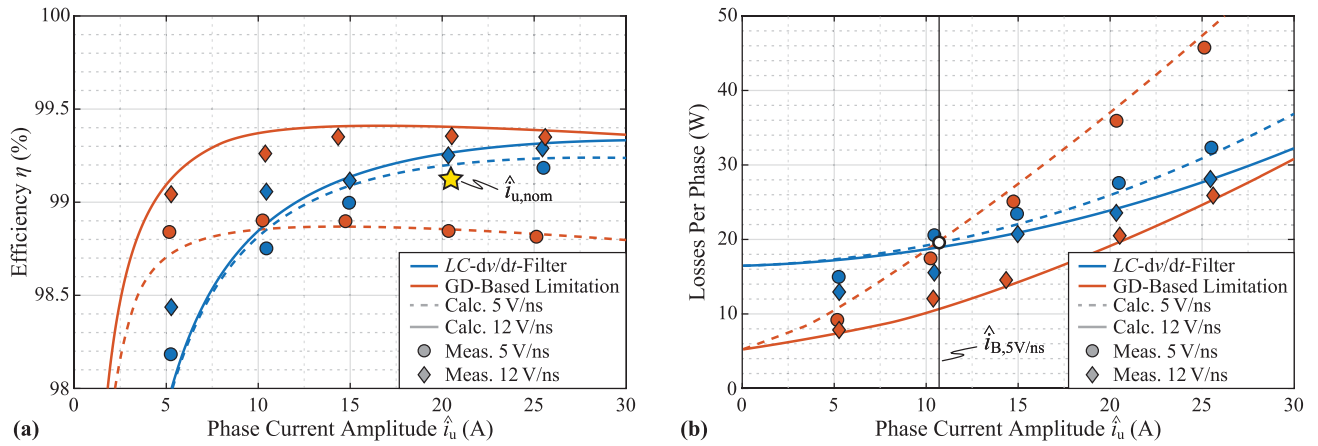
FIGURE 8. (a) Calculated (lines) and measured (circles/diamonds) efficiency and (b) losses per phase of the three-phase SiC-based VSD for the *LC*-dv/dt-filter (blue) and the GD-based limitation (orange) and two voltage slew rates dv/dt = 5 V/ns (dashed line, circles) and dv/dt = 12 V/ns (continuous lines, diamonds). The efficiency with *LC*-dv/dt-filter at 5 V/ns for nominal phase current $\hat{i}_u$ = 20.7 A is highlighted with ★.

between dv/dt = 5 V/ns (32.3 W for $\hat{i}_{u,max}$ = 25.9 A, i.e., η = 99.18 %) and dv/dt = 12 V/ns (28.1 W for $\hat{i}_{u,max}$ = 25.9 A, i.e., η = 99.29 %) as only the comparably low filter inductor conduction losses differ, whereas with GD-based limitation for the same current, the losses considerably increase for a low dv/dt (45.8 W for 5 V/ns and 25.9 W for 12 V/ns). This trend is also highlighted in Fig. 4 for the two exemplary voltage slew rates of 5 V/ns and 12 V/ns (thick circles / diamonds), to demonstrate that a higher efficiency (and power density) is achieved with the *LC*-dv/dt-filter for 5 V/ns, and with the GD-based limitation for dv/dt = 12 V/ns. A very interesting property of the GD-based dv/dt-limitation is the high part-load efficiency, since the main loss component (overlap losses) scales linearly with the switched current (and thus $\hat{i}_u$ and P_{out}), whereas the *LC*-dv/dt-filter has a constant loss offset P_{C_f}, which inherently degrades efficiency at low output power.

Therefore, in future traction applications allowing voltage slew rates above 10 V/ns, a GD-based dv/dt-limitation is favorably used considering full-load and part-load efficiency as well as functional volume. For state-of-the-art applications operating with low dv/dt-values of, e.g., 5 V/ns, an *LC*-dv/dt-filter typically offers higher efficiency and lower volume unless the required mission profile contains mainly part-load operation below 40 % of full-load ($\hat{i}_u$ < 10 A), in which case also for low dv/dt-values the GD-based limitation becomes more attractive.

D. THREE-PHASE VSD OPERATION WITH dv/dt-FILTER

Finally, the three-phase with operation of the VSD depicted in Fig. 5 connected to a state-of-the-art motor (Siemens 1FT7084 [26]) is verified. Considering the power level of 10 kW and a required the dv/dt-rating below typically 6 V/ns, the dv/dt-limitation is preferably realized with an *LC*-filter based on the theoretical findings from Fig. 6 and according to the experimental results in Fig. 8.
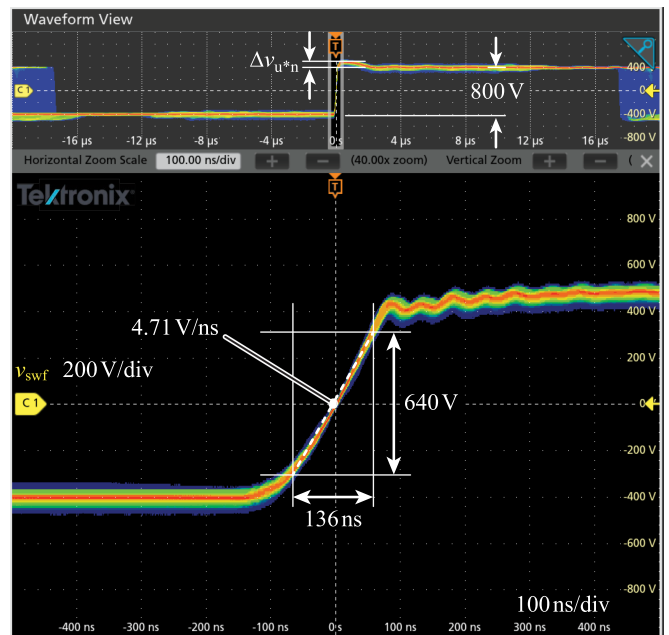

FIGURE 9. Measured voltage slew rate of the rising edge in phase u with the selected PMSM connected to the output. The effective machine capacitance slightly reduces the nominally set dv/dt (10 % to 90 % of V_{DC}) from 5.6 V/ns to 4.71 V/ns (approximately 15 % decrease). The small overshoot $\Delta v_{u*n} \approx 100$ V resulting from the finite filter resonance damping is further indicated.

Fig. 9 shows the measured voltage slew rate of > 1 million rising transitions of phase u (color-coded intensity grading) with the PMSM directly connected to the output (IMD). The measured dv/dt of 4.71 V/ns is lower than the nominally set 5.6 V/ns, which in a first approximation can be explained with an additional effective capacitance C_{add} at the filter output that influences the dv/dt according to

$$\left.\frac{dv}{dt}\right|_{new} = \left.\frac{dv}{dt}\right|_{nom} \cdot \frac{1}{\sqrt{1 + C_{add}/C_f}}. \quad (19)$$
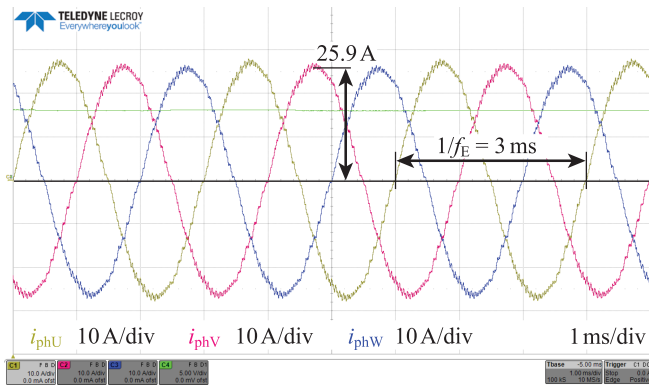
FIGURE 10. Three-phase machine currents of the 1FT7084 PMSM, demonstrating full-load capability ($\hat{i}_u = 25.9$ A) of the VSD.

An additional effective capacitance $C_{add} \approx 460$ pF explains the reduction of the dv/dt to 4.71 V/ns, where the machine itself contributes 300 pF as described in Section II-A, and the rest is attributed to component tolerances and impact of connections and PCB parasitics.

While it is true that the machine capacitance influences the set dv/dt and therefore, a fully machine-independent inverter and filter design is not possible, a lower than expected dv/dt is typically not critical, since it only reduces the detrimental effects of overvoltage, partial discharges and the like. At the same time, the *additional* losses (compared to operating the VSD without any LC-dv/dt-filter) are only defined by C_f and L_f and not the machine (the machine capacitance and - if present - the cable capacitance are anyway charged and discharged with the switching frequency, regardless of a dv/dt-limiting circuit). The impact of the load on the resulting voltage slew rate could obviously be minimized by increasing C_f, which, however, would directly increase the filter losses. Fig. 9 further indicates the slight voltage overshoot $\Delta v_{u*n} \approx 100$ V (12.5 % for $V_{DC} = 800$ V) resulting from the finite filter resonance damping with $C_{p,n}$, $D_{p,n}$ and $R_{p,n}$.

Fig. 10 shows the three phase currents of the VSD demonstrating operation at full load of $P_{M,max} = 10$ kW ($\hat{i}_u = \hat{i}_v = \hat{i}_w = 25.9$ A). For nominal load ($P_{M,nom} = 8$ kW with $\hat{i}_{u,nom} = 20.7$ A), measured overall system losses of $P_{loss,tot} = 580$ W and an efficiency of $\eta_{nom,tot} = \eta_{nom,VSD} \cdot \eta_{nom,PMSM} = 93.24$ % result (including the connected PMSM). Considering the nominal machine efficiency of 94 % [26], the overall VSD losses can be approximated with $P_{loss,VSD} \approx 70$ W and $\eta_{nom,VSD} = 99.19$ %, which agrees very well with the calculations and the experimental loss measurements (cf. the highlighted point with ★ in Fig. 8(a)).

V. CONCLUSION

SiC power MOSFETs are promising candidates to improve the efficiency and power density of electric motor-driven systems and further to promote the emerging trend of full integration of the inverter system into the motor housing. A primary advantage of SiC power semiconductors is their low specific switching losses that allow to design VSD inverter systems with considerably higher switching frequencies. This comes, however, at the expense of very fast voltage transients (high dv/dt). The voltage slew rate applied to the motor must be limited to prevent surge overvoltage, unequal voltage distribution across the windings or inadmissibly high bearing currents that all lead to accelerated aging and/or destruction of the motor. For a typical industry application of a 10 kW VSD operating primarily under part-load (80 % rated load), this article compares two approaches to limit the applied dv/dt, namely a passive LC-dv/dt-filter (single-stage LC-filter) and a GD-based dv/dt-limitation. While state-of-the-art motors demand voltage slew rates below typically 6 V/ns, future motors with reinforced insulation are forecasted to withstand a dv/dt of up to 15 V/ns, and therefore the question arises, which limiting concept is best-suited in a VSD for a certain dv/dt and phase current amplitude (full- or part-load).

The passive LC-dv/dt-filter mainly contributes a constant loss offset and low current/load dependent losses, whereas the GD-based limitation generates voltage-current overlap losses that scale linearly with output power and the voltage transition times. It turns out that the latter is best-suited for dv/dt-limits above 11 V/ns under full- and part-load operation. For each dv/dt-limit below 11 V/ns there exists a boundary for the phase current amplitude above which the LC-dv/dt-filter is preferably used, since the overlap losses of the GD-based limitation dominate the (roughly) constant losses of the filter. For part-load operation with a phase current amplitude below the boundary, however, the GD-based limitation has lower losses. In any case, it is possible to realize a VSD with an efficiency above 99 % for nominal load operation (8 kW). Similarly to the losses, the functional volume (considering the additional components as well as the required cooling to dissipate the additional losses) of the GD-based limitation is lower for high slew rates due to the lower losses compared to the LC-dv/dt-filter.

The theoretical findings are experimentally verified on an ultra-compact 10 kW tp SiC-based VSD as IMD for a state-of-the-art PMSM, which according to the findings of this work, features a passive LC-dv/dt-filter to limit the voltage slew rate to a nominal value of 5.6 V/ns. With a power density of 30 kW/dm^3 (493 W/in^3) it facilitates full integration of the inverter into the motor housing. The resulting measured dv/dt (4.71 V/ns) during operation with the PMSM is about 15 % lower than the nominal value, attributed to the additional capacitive loading from the PMSM, which slightly alters the filter corner frequency. Nevertheless, a dv/dt below the critical limit is non-problematic, as it further reduces the detrimental effects arising from fast voltage slew rates, while the losses are solely defined by the actual LC-filter components. The same system for a next-generation motor with higher dv/dt-rating would preferably be realized with a GD-based limitation, which not only reduces the total losses but also comes with an additional increase in power density, since no additional passive components must be placed. For Low-Voltage (LV) MOSFETs there exist already highly integrated "smart" GDs
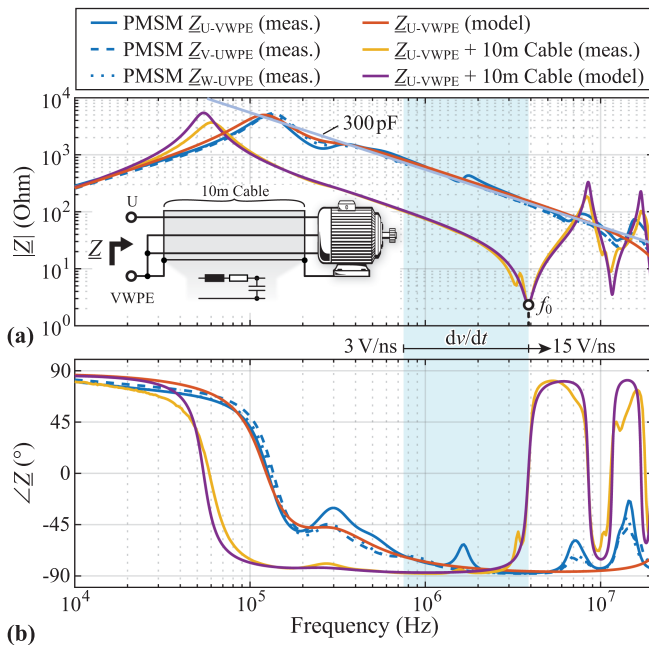
FIGURE 11. Impedance measurements $\underline{Z}_{U-VWPE}$ of the PMSM (blue) and comparison with the lumped-element model (orange). (a) Magnitude and (b) Phase. Further included is the impact of a 10 m shielded motor cable (yellow and purple). The frequency range of interest for the considered dv/dt-values is highlighted.

FIGURE 12. Lumped-element model of the PMSM characterizing the behavior seen between terminal U and the other two terminals V and W shorted to PE. Further indicated are the circuit element values.

L_{m1}	R_{p1}	C_{p1}	L_{m2}	R_{p2}	C_{p2}	L_{m3}	R_{m3}	C_{p3}
3.5 mH	4.6 kΩ	425 pF	584 µH	1 kΩ	378 pF	200 nH	3.5 Ω	60 pF

FIGURE 13. (a) Simulated dv/dt of the switched voltage in a VSD versus the nominally set value for the case of an unloaded LC-dv/dt-filter (blue), connected PMSM directly at the filter output (orange) and the PMSM connected via a 10 m long shielded motor cable (yellow). (b) The calculated additional effective capacitance C_{add} that yields the simulated dv/dt-values from (a).

that allow to actively (programmatically) set the voltage slew rates without influence of external parasitic effects [36] and it is very likely that in the near future similar concepts will be available for High-Voltage (HV) MOSFETs ($\geq$ 1.2 kV blocking voltage capability).

APPENDIX

In this Appendix the considered PMSM is characterized with impedance measurements and an intuitive, physically explainable lumped-element equivalent circuit is derived to justify the capacitor selection in the LC-dv/dt-filter design. From (4) follows a filter resonance frequency range between 760 kHz and 3.8 MHz for a dv/dt-limitation range between 3 V/ns and 15 V/ns. The impact of the machine on the voltage slew rate can be quantified with a model that is valid in this frequency range. Based on impedance measurements between one machine terminal (e.g., U) and the remaining two terminals (shorted to PE, e.g., $VWPE$) as depicted with the blue curves in Fig. 11, the lumped-element circuit model of Fig. 12 with indicated component values results. The first and second parallel resonances at around 130 kHz and 340 kHz, respectively, are modeled with L_{m1} and C_{p1} (damping R_{p1}) and L_{m2} and C_{p2} (damping R_{p2}). The damped series resonance in between is composed of the combination of the six elements. The final series resonance at around 25 MHz (not visible in the measurements of Fig. 11) is modeled with L_{m3} and the series connection of C_{p1} and C_{p2} (damping R_{m3}). Finally, the capacitive coupling from the terminals and windings to the housing (PE) is modeled with the capacitance C_{p3}. Despite its simple structure and the absence of frequency dependent
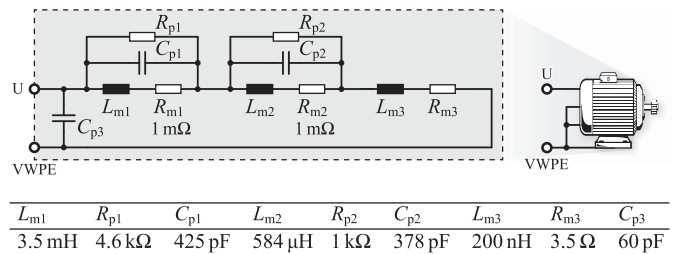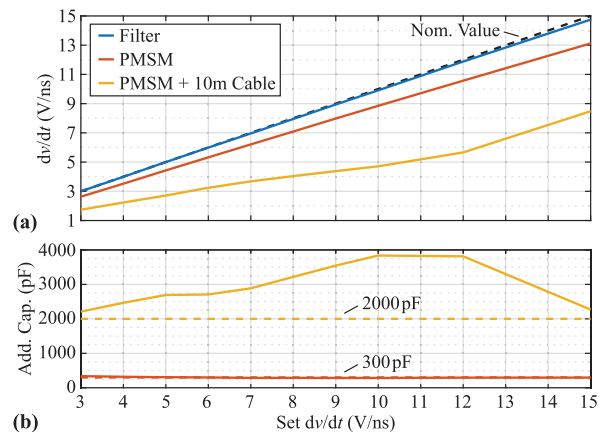
machine inductances and resistances that would be required for accurate high-frequency characterization in the multi-ten-MHz range [19], this model accurately replicates the PMSM impedance in the frequency range of interest up to approximately 4 MHz (highlighted in light blue in Fig. 11). Observing the almost entirely capacitive nature of $\underline{Z}_{U-VWPE}$ in the highlighted frequency range of interest, the approximation of the PMSM impedance as single 300 pF capacitance from Section II-A to facilitate the filter design is therefore justified.

Fig. 11 further highlights the impact of a 10 m long shielded motor cable (Siemens 6FX5002-5DN56-1BA0) on the resultant impedance $\underline{Z}_{U-VWPE}$ (measurement: yellow). For the calculation model (purple curve), the cable is treated as series of ten distributed RLC-elements with 0.35 Ω, 154 nH, 170 pF each. In the highlighted frequency range the simplified approximation with a constant capacitance (2 nF; 1.7 nF from the 10 m cable and 300 pF from the PMSM) is clearly not valid anymore, since the first cable resonance occurs at 4 MHz, characterized by a drastic drop of the impedance. This is manifested in Fig. 13(a) that shows the simulated dv/dt of a voltage transient in one of the VSD bridge-legs compared to the set nominal values (C_{filt} = 1.12 nF and L_{filt} resulting from (4)) in case of the unloaded filter (no machine; blue), a connected PMSM without motor cable (orange) and

a PMSM connected via a 10 m long shielded motor cable (yellow). Fig. 13(b) nicely shows that in case of a connected PMSM without motor cable the dv/dt-reduction below the set value can be explained with the additional effective machine capacitance of 300 pF calculated according to (19). If in addition a 10 m long motor cable is added, the resulting "cable-PMSM"-behavior is not purely capacitive anymore in the frequency range of interest, and the calculated additional capacitance to get the dv/dt from the yellow curve in Fig. 13 (a) is larger than the theoretical 2 nF (cable + PMSM) due to the "cable-PMSM" resonance that is located close to the filter resonance frequency. In any case, the dv/dt is always lower than the nominally set value and therefore allows safe operation of the machine.

REFERENCES

[1] M. Haider, M. Guacci, D. Bortis, J. W. Kolar, and Y. Ono, "Analysis and evaluation of active/hybrid/passive DV/DT-filter concepts for next generation SiC-based variable speed drive inverter systems," in *Proc. IEEE Energy Convers. Congr. Expo.*, Detroit, MI, USA, 2020, pp. 4923–4930.

[2] P. Waide and C. U. Brunner, "Energy-efficiency policy opportunities for electric motor-driven systems," *Int. Energy Agency*, pp. 11–45, 2011.

[3] Nidec Corporation, "Energy efficiency," acim.nidec.com. Accessed: Feb. 27, 2023. [Online]. Available: https://acim.nidec.com/motors/usmotors/energy-efficiency

[4] K. Shirabe et al., "Advantages of high frequency PWM in AC motor drive applications," in *Proc. IEEE Energy Convers. Congr. Expo.*, Raleigh, NC, USA, 2012, pp. 2977–2984.

[5] M. Slawinski, D. Heer, T. Villbusch, and M. Buschkuehle, "System study of SiC MOSFET and si IGBT power module performance using a bidirectional buck-boost converter as evaluation platform," in *Proc. 18th Eur. Conf. Power Electron. Appl.*, Karlsruhe, Germany, 2016, pp. 1–8.

[6] T. Bürger, K. Berberich, and S. Prüfling, "Silicon carbide semiconductors for the e-powertrain," *ATZ Elektron Worldwide*, vol. 13, pp. 48–51, 2018.

[7] L. Zhang, X. Yuan, X. Wu, C. Shi, J. Zhang, and Y. Zhang, "Performance evaluation of high-power SiC MOSFET modules in comparison to si IGBT modules," *IEEE Trans. Power Electron.*, vol. 34, no. 2, pp. 1181–1196, Feb. 2019.

[8] Q. Yan, X. Yuan, Y. Geng, A. Charalambous, and X. Wu, "Performance evaluation of split output converters with SiC MOSFETs and SiC schottky diodes," *IEEE Trans. Power Electron.*, vol. 32, no. 1, pp. 406–422, Jan. 2017.

[9] T. M. Jahns and B. Sarlioglu, "The incredible shrinking motor drive: Accelerating the transition to integrated motor drives," *IEEE Power Electron. Mag.*, vol. 7, no. 3, pp. 18–27, Sep. 2020.

[10] ABB Industrial Systems, "Effects of AC drives on motor insulation - knocking down the standing wave," Technical Guide Number 102, Apr. 1998.

[11] S. Sundeep, J. Wang, A. Griffo, and F. Alvarez-Gonzalez, "Antiresonance phenomenon and peak voltage stress within PWM inverter fed stator winding," *IEEE Trans. Ind. Electron.*, vol. 68, no. 12, pp. 11826–11836, Dec. 2021.

[12] S. Sundeep, J. Wang, and A. Griffo, "Holistic modeling of high-frequency behavior of inverter-fed machine winding, considering mutual couplings in time domain," *IEEE Trans. Ind. Appl.*, vol. 57, no. 6, pp. 6044–6057, Nov. 2021.

[13] M.-M. Bakran, "High DV/DT and the challenges on device and motor," in *Proc. Workshop ECPE SiC GaN User Forum*, Munich, Germany, 2019, pp. 1–28.

[14] J. Erdman, R. Kerkman, D. Schlegel, and G. Skibinski, "Effect of PWM inverters on AC motor bearing currents and shaft voltages," *IEEE Trans. Ind. Appl.*, vol. 32, no. 2, pp. 250–259, Mar. 1996.

[15] A. Schroedermeier and D. C. Ludois, "Integrated inductors, capacitors, and damping in bus bars for DV/DT filter applications," in *Proc. IEEE Appl. Power Electron. Conf. Expo.* San Antonio, TX, USA, 2018, pp. 2650–2657.

[16] J. He, J. Sabate, M. Schutten, Y. Singh, and Z. Zhang, "Design issues for high-power and high-performance SiC converters," *Proc. Tutorial IEEE Appl. Power Electron. Conf. Expo.*, Anaheim, CA, USA, 2019, pp. 1–28.

[17] NEMA (National Electrical Manufacturers Association), Motors and Generators, NEMA MG 1, 2021.

[18] *Rotating Electrical Machines - Part 18-41*, IEC 60034, International Electrotechnical Commission, Geneva, Switzerland, Jun. 2014.

[19] M. T. Fard, J. He, M. Sadoughi, B. Mirafzal, and F. Fateh, "Smart coils for mitigation of motor reflected overvoltage fed by SiC drives," in *Proc. IEEE Appl. Power Electron. Conf. Expo.*), Orlando, FL, USA, 2023, pp. 1429–1436.

[20] S.-J. Kim and S.-K. Sul, "A novel filter design for suppression of high voltage gradient in voltage-fed PWM inverter," in *Proc. IEEE Appl. Power Electron. Conf. Expo.* Atlanta, GA, USA, 1997, pp. 122–127.

[21] B. A. Acharya and V. John, "Design of output DV/DT filter for motor drives," in *Proc. 5th Int. Conf. Ind. Inf. Syst.*, Mangalore, India, 2010, pp. 562–567.

[22] M. Haider et al., "Analytical calculation of the residual ZVS losses of TCM-operated single-phase PFC rectifiers," *IEEE Open J. Power Electron.*, vol. 2, pp. 250–264, 2021.

[23] M. Haider, S. Fuchs, G. Zulauf, D. Bortis, J. W. Kolar, and Y. Ono, "Analytical loss model for three-phase 1200V SiC MOSFET inverter drive system utilizing miller capacitor-based DV/DT-limitation," *IEEE Open J. Power Electron.*, vol. 3, pp. 93–104, 2022.

[24] D. A. Rendusara and P. N. Enjeti, "An improved inverter output filter configuration reduces common and differential modes DV/DT at the motor terminals in PWM drive systems," *IEEE Trans. Power Electron.*, vol. 13, no. 6, pp. 1135–1143, Nov. 1998.

[25] J. He et al., "Multi-domain design optimization of DV/DT filter for SiC-based three-phase inverters in high-frequency motor-drive applications," *IEEE Trans. Ind. Appl.*, vol. 55, no. 5, pp. 5214–5222, Sep. 2019.

[26] Siemens, "SIMOTICS S-1FT7," Datasheet, May 2023.

[27] A. Schwaiger, "Reduce motor EMI & insulation voltage stress with slew rate control gate driver," *Broadcom*, pp. 1–20, 2022.

[28] H. Kim, S. Acharya, A. Anurag, B.-H. Kim, and S. Bhattacharya, "Effect of inverter output DV/DT with respect to gate resistance and loss comparison with DV/DT filters for SiC MOSFET based high speed machine drive applications," in *Proc. IEEE Energy Convers. Congr. Expo.*, Baltimore, MD, USA, 2019, pp. 2301–2306.

[29] A. P. Camacho, V. Sala, H. Ghorbani, and J. L. R. Martinez, "A novel active gate driver for improving SiC MOSFET switching trajectory," *IEEE Trans. Ind. Electron.*, vol. 64, no. 11, pp. 9032–9042, Nov. 2017.

[30] Y. Lobsiger and J. W. Kolar, "Closed-loop IGBT gate drive featuring highly dynamic DI/DT and DV/DT control," in *Proc. IEEE Energy Convers. Congr. Expo.*, Raleigh, NC, USA, 2012, pp. 4754–4761.

[31] S. Beushausen, F. Herzog, and R. W. D. Doncker, "GaN-based active gate-drive unit with closed-loop DU/DT-control for IGBTs in medium-voltage applications," in *Proc. Power Convers. Intell. Motion Conf.* 2020, pp. 1–8.

[32] M. Guacci et al., "Experimental characterization of silicon and gallium nitride 200V power semiconductors for modular/multi-level converters using advanced measurement techniques," *IEEE Trans. Emerg. Sel. Topics Power Electron.*, vol. 8, no. 3, pp. 2238–2254, Sep. 2020.

[33] Cree, "C3M0016120K - silicon carbide power MOSFET," Datasheet, Apr. 2019.

[34] U. Drofenik, G. Laimer, and J. W. Kolar, "Theoretical converter power density limits for forced convection cooling," in *Proc. Power Convers. Intell. Motion Conf.*, 2005, pp. 608–619.

[35] G. Rohner, J. W. Kolar, and D. Bortis, "Optimal level number and performance evaluation of GaN/Si multi-level flying capacitor inverter for variable speed drive systems," in *Proc. 25th Int. Conf. Elect. Machines Syst.*, Chiang Mai, Thailand, 2022, pp. 1–8.

[36] Infineon, "MOTIX 6EDL7141 - 3 Phase Smart Gate Driver, Datasheet, Sep. 2022.